Supplementary Information

Coordination Engineering in Single-atom Covalent Organic Frameworks Photocatalysts for Solar-Driven Nitrogen Fixation

Weiguo Li [†a,b], Helong Wu[†b], Liangchun Wu[b], Yuan Hu[b], Yuansong Ye[b], Diwen Liu[c], Dejing Li[b], Yanjie Zhang[b], Zuju Ma[d], Rongjian Sa*[a,b]

[a]College of Materials Science and Engineering, Fujian Normal University, Fuzhou 350007, China

[b]Fujian Key Laboratory of Functional Marine Sensing Materials, College of Materials and Chemical Engineering, Minjiang University, Fuzhou, Fujian, 350108, China. Email: rjsa@mju.edu.cn

[c]School of Materials and Chemical Engineering, Pingxiang University, Pingxiang 337055, China

[d]School of Environmental and Materials Engineering, Yantai University, Yantai, 264005, China

Table S1. Binding Energy (E_b) and Cohesive Energy (E_c) of TM@pdiCOF (TM = Fe, Co or Ni).

	E_b (eV)	E_c (eV)	$E_b - E_c$ (eV)
Fe	-9.25	-5.11	-4.14
Co	-9.82	-5.22	-4.59
Ni	-12.90	-5.45	-7.45

Table S2. Binding Energy (E_b) and Cohesive Energy (E_c) of TM@NpdiCOF, TM@2NpdiCOF and TM@3NpdiCOF (TM = Fe, Co or Ni).

		E_b (eV)	$E_b - E_c$ (eV)
Fe	Fe@NpdiCOF	-9.85983	-4.748
	Fe@2NpdiCOF	-9.61187	-4.500
	Fe@3NpdiCOF	-9.91038	-4.799
Co	Co@NpdiCOF	-10.3055	-5.085
	Co@2NpdiCOF	-10.0880	-4.868
	Co@3NpdiCOF	-10.2095	-4.989
Ni	Ni@NpdiCOF	-11.8156	-6.363
	Ni@2NpdiCOF	-11.7069	-6.254
	Ni@3NpdiCOF	-11.4446	-5.992

Table S3. N≡N bond length in nitrogen of TM@NpdiCOF, TM@2NpdiCOF and TM@3NpdiCOF (TM = Fe, Co or Ni).

		End-on (Å)	Side-on (Å)
Fe	Fe@NpdiCOF	1.142	1.167
	Fe@2NpdiCOF	1.141	1.171
	Fe@3NpdiCOF	1.144	1.185
Co	Co@NpdiCOF	1.138	1.160
	Co@2NpdiCOF	1.138	1.160
	Co@3NpdiCOF	1.138	1.174
Ni	Ni@NpdiCOF	1.134	1.154
	Ni@2NpdiCOF	1.135	1.159
	Ni@3NpdiCOF	1.139	1.178

Table S4. Fractional atomistic coordinates of TM@pdiCOF. Space group P1, a = 30.380 Å, b = 30.380 Å, c = 7.000 Å, α = γ = 90.000°, and β = 120.000 °.

Atom	x	y	z
C1	0.9500	0.6991	0.5000
C2	0.9494	0.7494	0.5000
C3	0.9003	0.6475	0.5000
C4	0.6601	0.3805	0.5000
C5	0.7138	0.3870	0.5000
C6	0.5594	0.3204	0.5000
C7	0.7550	0.4881	0.5000
C8	0.8026	0.5416	0.5000
C9	0.8560	0.5474	0.5000
C10	0.8617	0.4999	0.5000
C11	0.8143	0.4465	0.5000
C12	0.3009	0.2510	0.5000
C13	0.2506	0.2000	0.5000
C14	0.3525	0.2527	0.5000
C15	0.6195	0.2797	0.5000
C16	0.6130	0.3268	0.5000
C17	0.6796	0.2390	0.5000
C18	0.5119	0.2670	0.5000
C19	0.4584	0.2610	0.5000
C20	0.4526	0.3086	0.5000
C21	0.5002	0.3619	0.5000
C22	0.5535	0.3678	0.5000
C23	0.7490	0.0500	0.5000
C24	0.8000	0.0506	0.5000
C25	0.7473	0.0997	0.5000
C26	0.7203	0.3399	0.5000
C27	0.6732	0.2862	0.5000
C28	0.7610	0.4406	0.5000
C29	0.7330	0.2450	0.5000
C30	0.7390	0.1974	0.5000
C31	0.6914	0.1440	0.5000
C32	0.6381	0.1383	0.5000
C33	0.6322	0.1857	0.5000
C34	0.6991	0.9500	0.5000
C35	0.6475	0.9003	0.5000
C36	0.7494	0.9494	0.5000
C37	0.3805	0.6601	0.5000
C38	0.3870	0.7138	0.5000
C39	0.3204	0.5594	0.5000

C40	0.4881	0.7550	0.5000
C41	0.5416	0.8026	0.5000
C42	0.5474	0.8560	0.5000
C43	0.4999	0.8617	0.5000
C44	0.4465	0.8143	0.5000
C45	0.2510	0.3009	0.5000
C46	0.2000	0.2506	0.5000
C47	0.2527	0.3525	0.5000
C48	0.2797	0.6195	0.5000
C49	0.3268	0.6130	0.5000
C50	0.2390	0.6796	0.5000
C51	0.2670	0.5119	0.5000
C52	0.2610	0.4584	0.5000
C53	0.3086	0.4526	0.5000
C54	0.3619	0.5002	0.5000
C55	0.3678	0.5535	0.5000
C56	0.0500	0.7490	0.5000
C57	0.0506	0.8000	0.5000
C58	0.0997	0.7473	0.5000
C59	0.3399	0.7203	0.5000
C60	0.2862	0.6732	0.5000
C61	0.4406	0.7610	0.5000
C62	0.2450	0.7330	0.5000
C63	0.1974	0.7390	0.5000
C64	0.1440	0.6914	0.5000
C65	0.1383	0.6381	0.5000
C66	0.1857	0.6322	0.5000
C67	0.0000	0.8002	0.5000
C68	0.1998	0.1998	0.5000
C69	0.8002	0.0000	0.5000
N1	0.9032	0.5993	0.5000
N2	0.4006	0.3039	0.5000
N3	0.6961	0.0968	0.5000
N4	0.5993	0.9032	0.5000
N5	0.3039	0.4006	0.5000
N6	0.0968	0.6961	0.5000
N7	0.6954	0.0000	0.5000
N8	0.0000	0.6954	0.5000
N9	0.3046	0.3046	0.5000
H1	0.9117	0.7491	0.5000
H2	0.8619	0.6457	0.5000
H3	0.6553	0.4153	0.5000
H4	0.7155	0.4836	0.5000
H5	0.7982	0.5767	0.5000

H6	0.9012	0.5042	0.5000
H7	0.8187	0.4114	0.5000
H8	0.2509	0.1626	0.5000
H9	0.3543	0.2161	0.5000
H10	0.5847	0.2400	0.5000
H11	0.5164	0.2319	0.5000
H12	0.4233	0.2215	0.5000
H13	0.4958	0.3970	0.5000
H14	0.5886	0.4073	0.5000
H15	0.8374	0.0883	0.5000
H16	0.7839	0.1381	0.5000
H17	0.7600	0.3447	0.5000
H18	0.7681	0.2845	0.5000
H19	0.7785	0.2018	0.5000
H20	0.6029	0.0988	0.5000
H21	0.5927	0.1813	0.5000
H22	0.7491	0.9117	0.5000
H23	0.6457	0.8619	0.5000
H24	0.4153	0.6553	0.5000
H25	0.4836	0.7155	0.5000
H26	0.5767	0.7982	0.5000
H27	0.5042	0.9012	0.5000
H28	0.4114	0.8187	0.5000
H29	0.1626	0.2509	0.5000
H30	0.2161	0.3543	0.5000
H31	0.2400	0.5847	0.5000
H32	0.2319	0.5164	0.5000
H33	0.2215	0.4233	0.5000
H34	0.3970	0.4958	0.5000
H35	0.4073	0.5886	0.5000
H36	0.0883	0.8374	0.5000
H37	0.1381	0.7839	0.5000
H38	0.3447	0.7600	0.5000
H39	0.2845	0.7681	0.5000
H40	0.2018	0.7785	0.5000
H41	0.0988	0.6029	0.5000
H42	0.1813	0.5927	0.5000
H43	0.8378	0.0000	0.5000
H44	0.0000	0.8378	0.5000
H45	0.1622	0.1622	0.5000
TM1	0.6500	0.0000	0.5000
TM2	0.0000	0.6500	0.5000
TM3	0.3501	0.3501	0.5000

Table S5. Comparison of Different NRR Catalysts[1-6]

Catalyst Type	Specific System	Limiting Potential (U_L)	NH_3 Yield	Reference
COF	WPc-TFPN	-0.19 V		1
COF	Re@TT-COF	-0.30 V		2
MOF	Fe_1-N-C	-0.05 V	1.56×10^{-11}mol cm^{-2} s^{-1}	3
Carbon-based SACs	Mo/melon	-0.36 V		4
Carbon-based SACs	CrN_4	-0.70 V		5
Carbon-based SACs	$MoNC_2$	-0.82 V		6

Table S6. Comparison of Different Catalyst Performances

	Fe@pdiCOF		Co@pdiCOF		Ni@pdiCOF	
	End-on	Side-on	End-on	Side-on	End-on	Side-on
d-band center	-2.64		-0.86		-2.26	
ΔG_{N2} (eV)	-1.74	-1.63	-2.96	-2.46	-0.84	-0.08
Charge Transfer (e^-)	0.49	0.54	0.37	0.44	0.27	0.32

Table S7. Comparison of N_2 adsorption energies calculated with different vdW correction methods.

System	Adsorption mode	DFT-D3	DFT-D2	optB86b-vdW
Fe@NpdiCOF	end-on	-0.89	-0.81	-0.71
	side-on	-1.54	-1.49	-1.33
Co@3NpdiCOF	end-on	-1.05	-1.79	-0.77
	side-on	-1.83	-1.80	-1.36
Ni@2NpdiCOF	end-on	-0.72	-0.85	-0.38
	side-on	-1.15	-0.85	-0.87

Table S8. Comparison of band gaps calculated with PBE, HSE06, and DFT+U for representative catalysts.

System	PBE	HSE06	DFT+U
Fe@NpdiCOF	0.307	1.368	0.514 (U = 4.5 eV)
Co@3NpdiCOF	0.390	1.326	0.867 (U = 3.3 eV)
Ni@2NpdiCOF	0.393	2.107	1.486 (U = 6.4 eV)

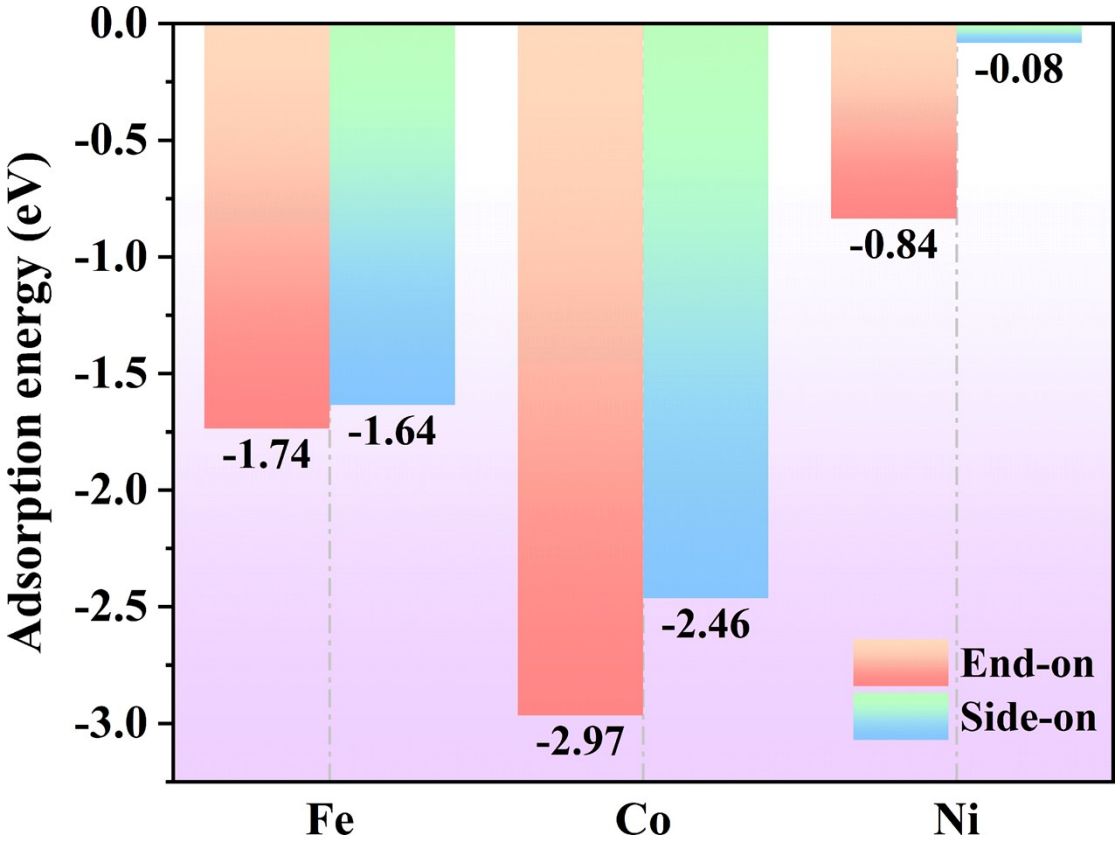

Figure S1. Adsorption energy (E_{ads}) of N_2 adsorbed on TM@pdiCOF (TM = Fe, Co or Ni).

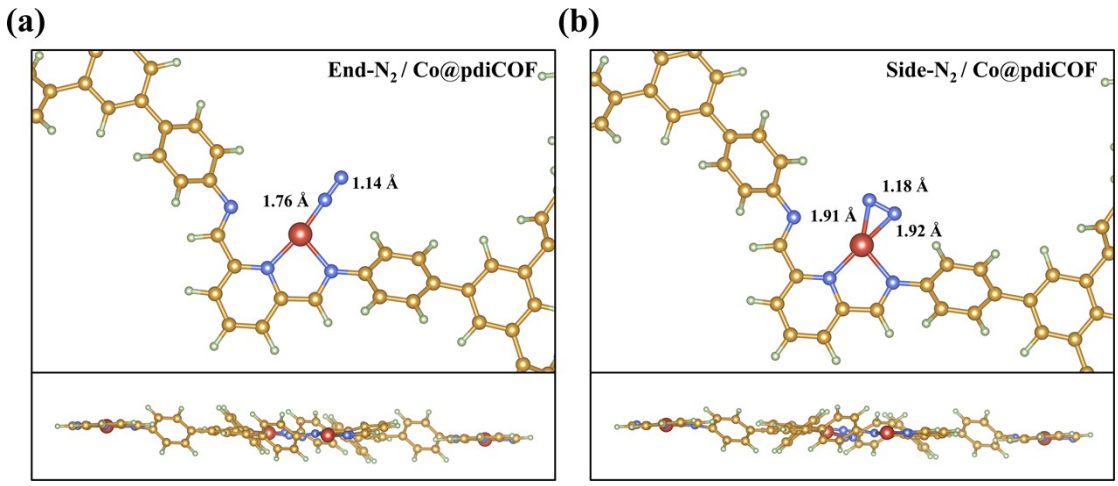

Figure S2. Optimized geometries for end-on (a) and side-on (b) adsorption of N_2 on Co@pdiCOF.

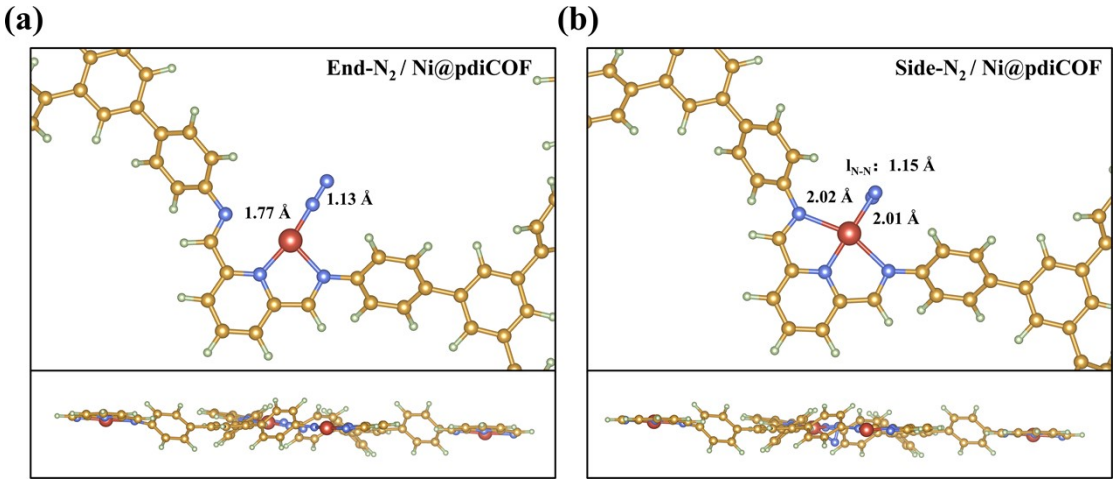

Figure S3. Optimized geometries for end-on (a) and side-on (b) adsorption of N_2 on Ni@pdiCOF.

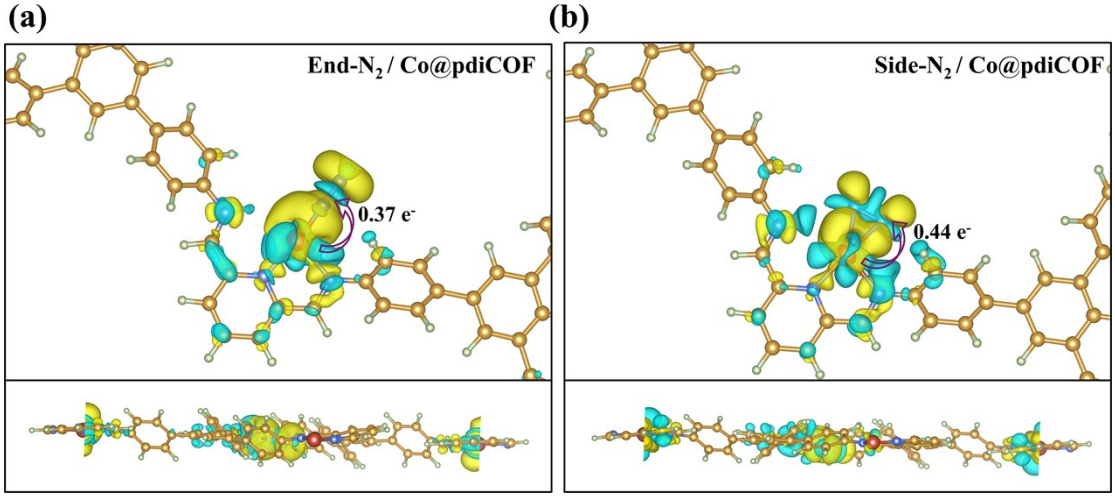

Figure S4. The charge density difference plot for N_2 in "end-on" (a) and "side-on" (b) adsorption on Co@pdiCOF. Isosurface level is taken as 0.001 eÅ^{-3}.

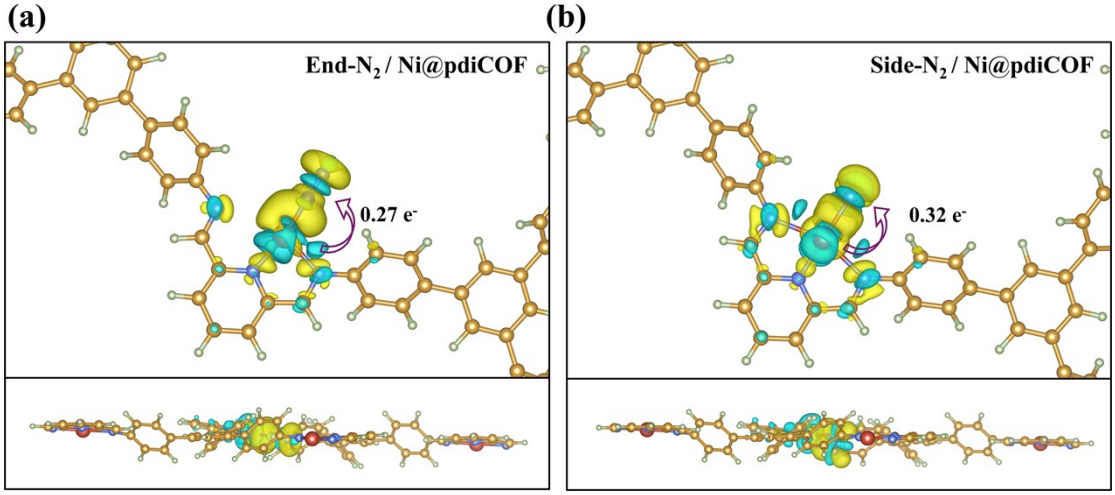

Figure S5. The charge density difference plot for N_2 in "end-on" (a) and "side-on" (b) adsorption on Ni@pdiCOF. Isosurface level is taken as 0.001 eÅ^{-3}.

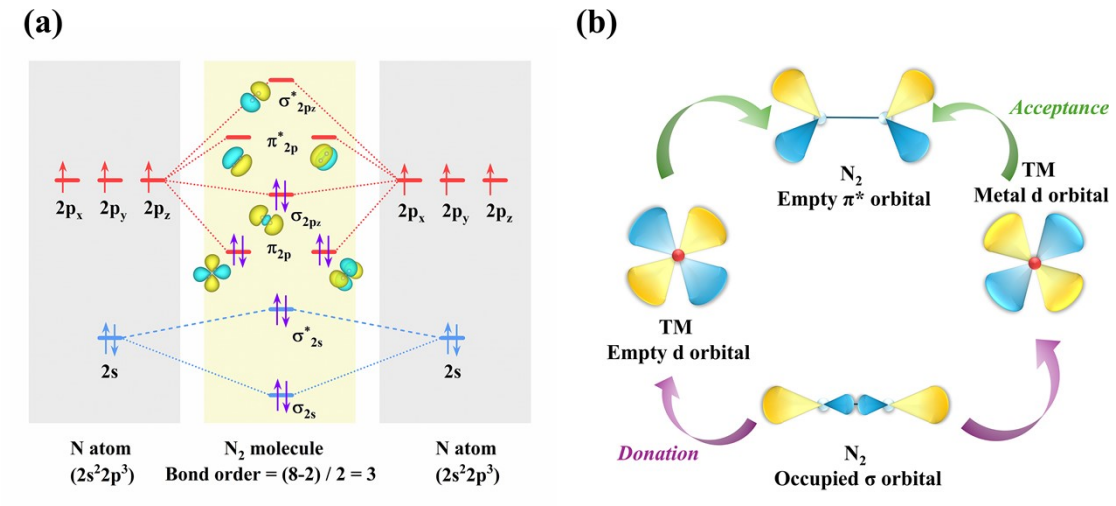

Figure S6. (a) Orbital hybridization diagrams of the free N_2 molecules, (b) Schematic Diagram of the "Donation-Acceptance" Mechanism.

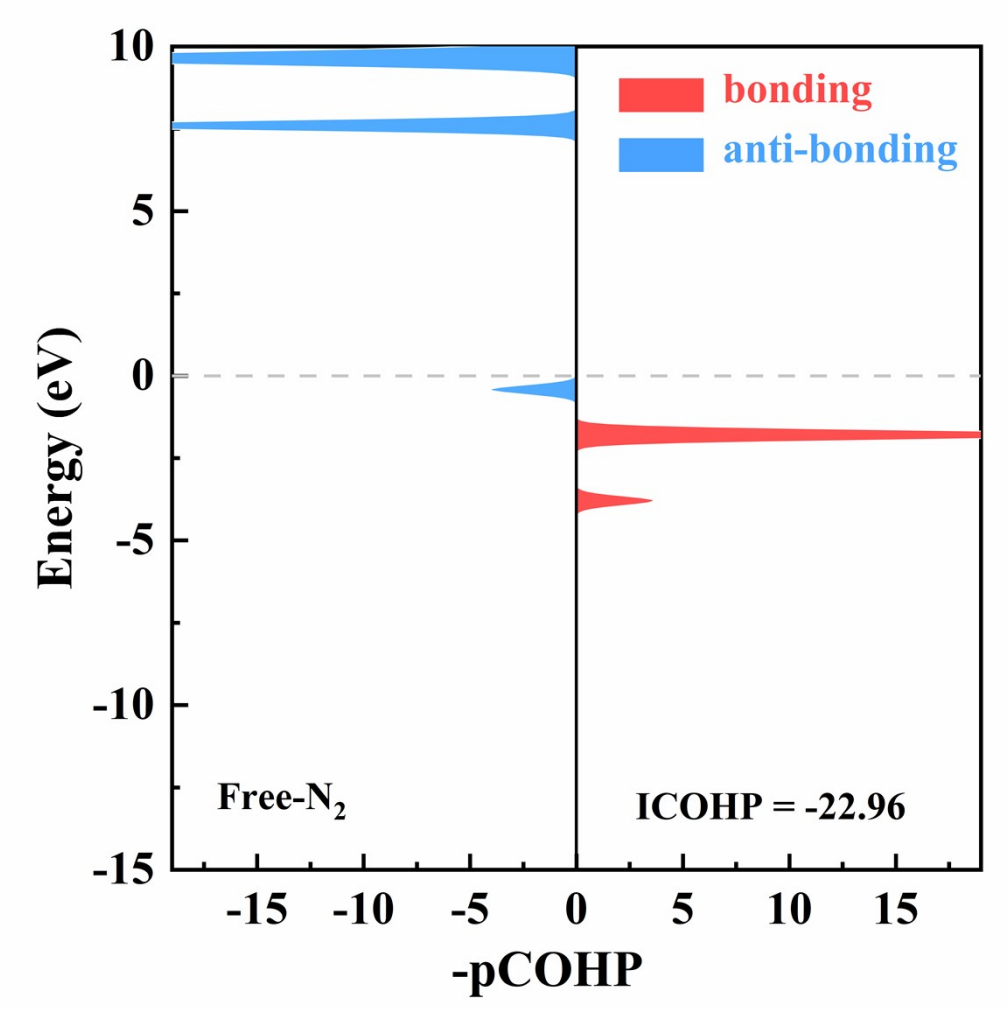

Figure S7. Projected Crystal Orbital Hamilton Population (-pCOHP) of N≡N interactions in free N_2. The Fermi level is set to be 0 eV.

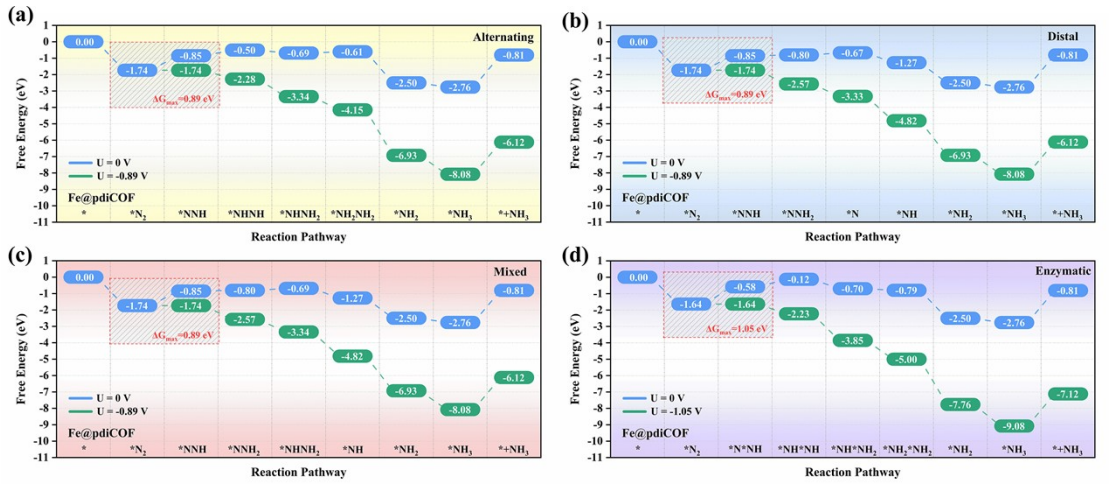

Figure S8. Free energy diagram of Fe@pdiCOF in NRR along (a) Alternating pathway, (b) Distal pathway, (c) Mixed pathway and (d) Enzymatic pathway.

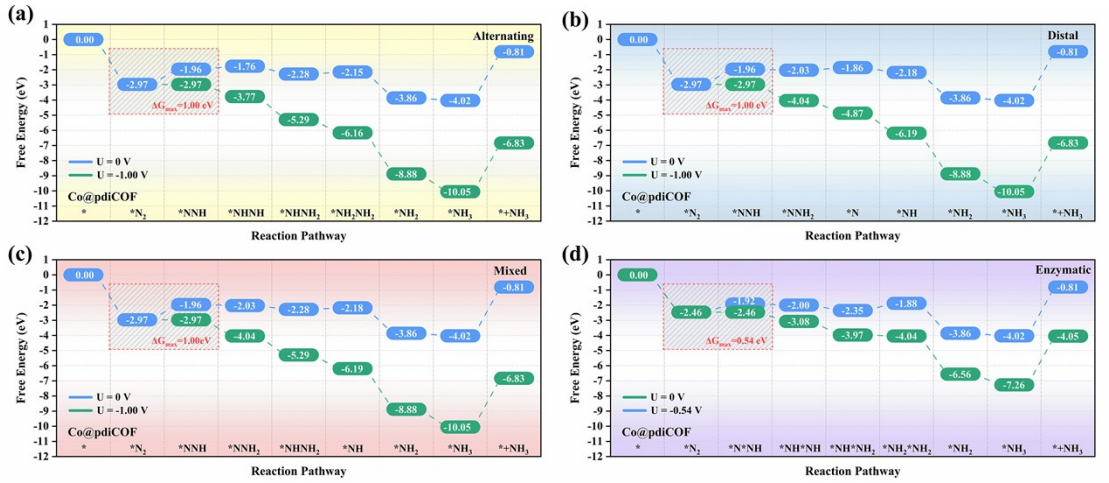

Figure S9. Free energy diagram of Co@pdiCOF in NRR along (a) Alternating pathway, (b) Distal pathway, (c) Mixed pathway and (d) Enzymatic pathway.

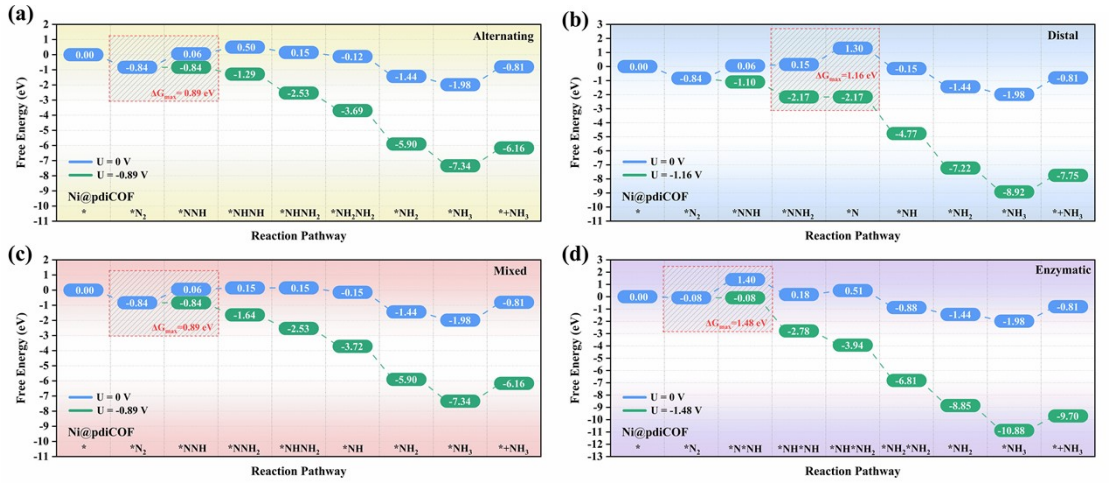

Figure S10. Free energy diagram of Ni@pdiCOF in NRR along (a) Alternating pathway, (b) Distal pathway, (c) Mixed pathway and (d) Enzymatic pathway.

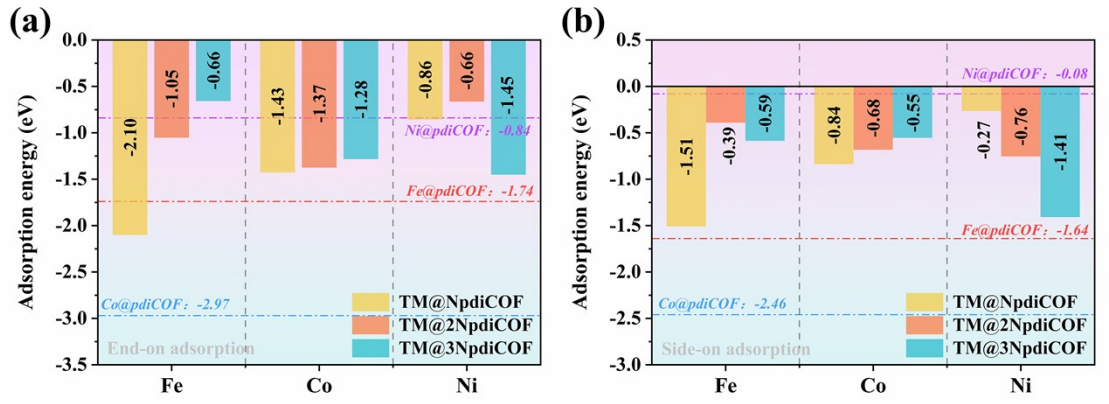

Figure S11. Adsorption energies of nitrogen adsorbed in (a) "End-on" and (b) "Side-on" configurations on TM@NpdiCOF, TM@2NpdiCOF, and TM@3NpdiCOF, where TM = Fe, Co and Ni.

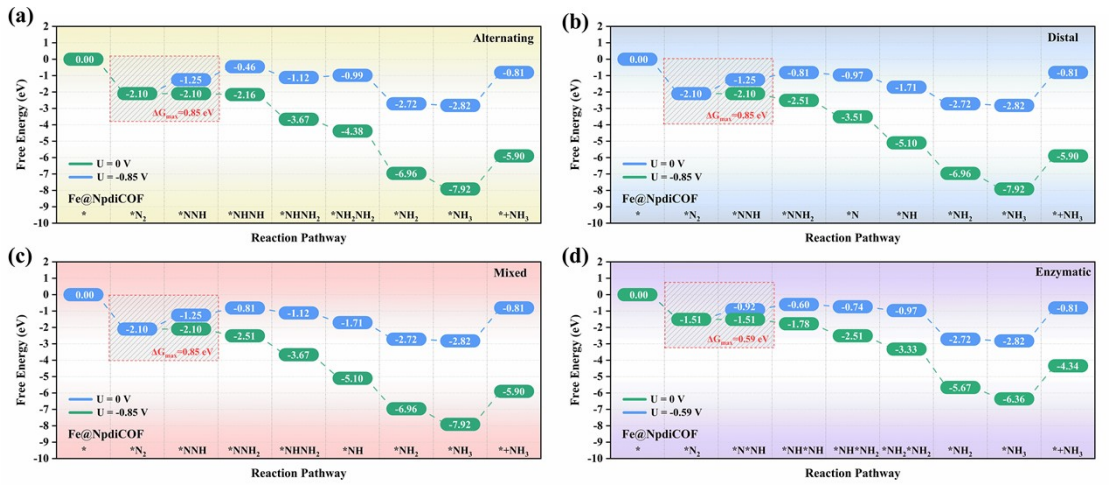

Figure S12. Free energy diagram of Fe@NpdiCOF in NRR along (a) Alternating pathway, (b) Distal pathway, (c) Mixed pathway and (d) Enzymatic pathway.

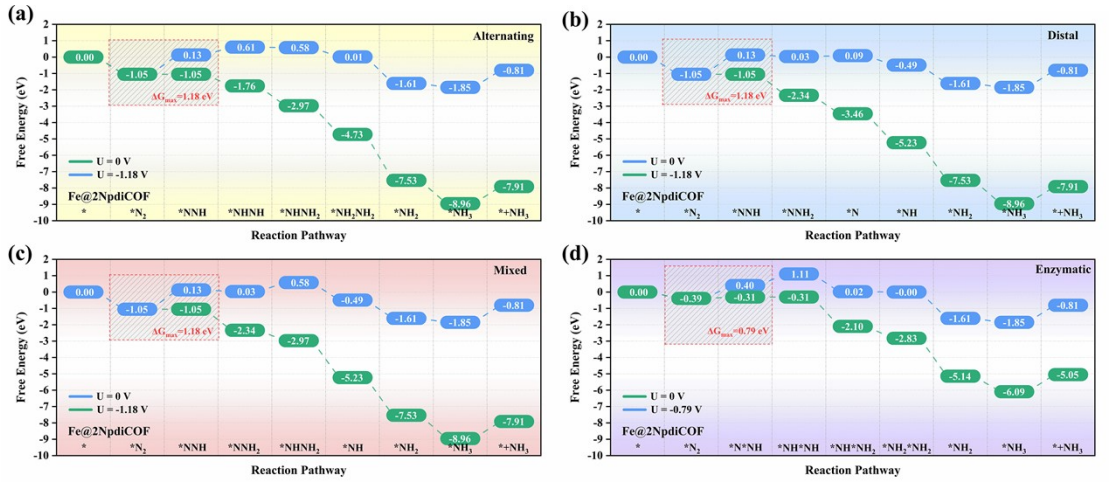

Figure S13. Free energy diagram of Fe@2NpdiCOF in NRR along (a) Alternating pathway, (b) Distal pathway, (c) Mixed pathway and (d) Enzymatic pathway.

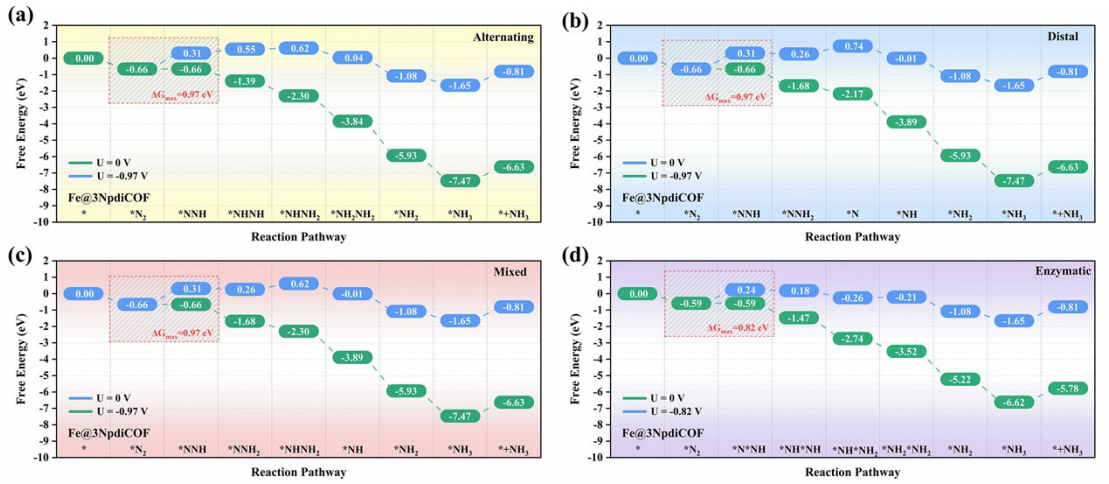

Figure S14. Free energy diagram of Fe@3NpdiCOF in NRR along (a) Alternating pathway, (b) Distal pathway, (c) Mixed pathway and (d) Enzymatic pathway.

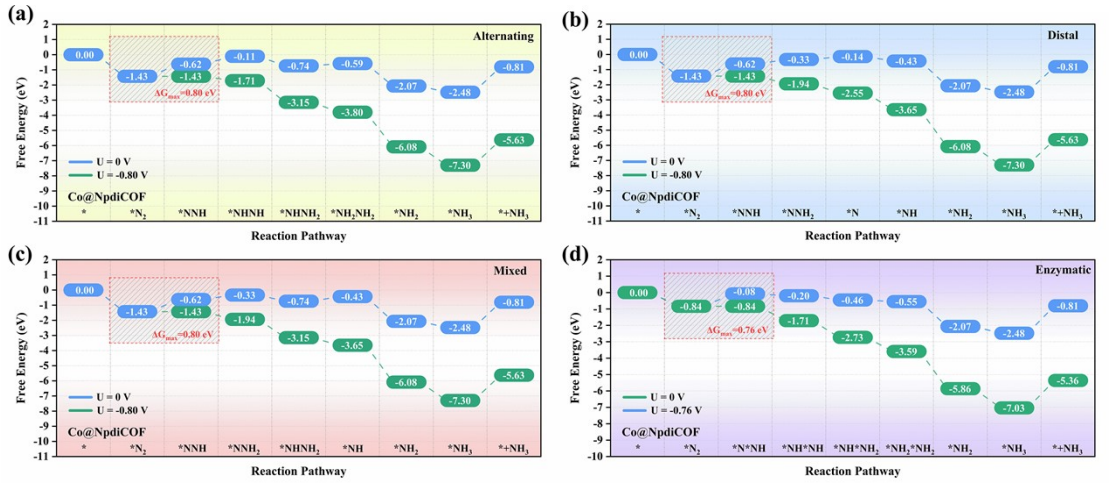

Figure S15. Free energy diagram of Co@NpdiCOF in NRR along (a) Alternating pathway, (b) Distal pathway, (c) Mixed pathway and (d) Enzymatic pathway.

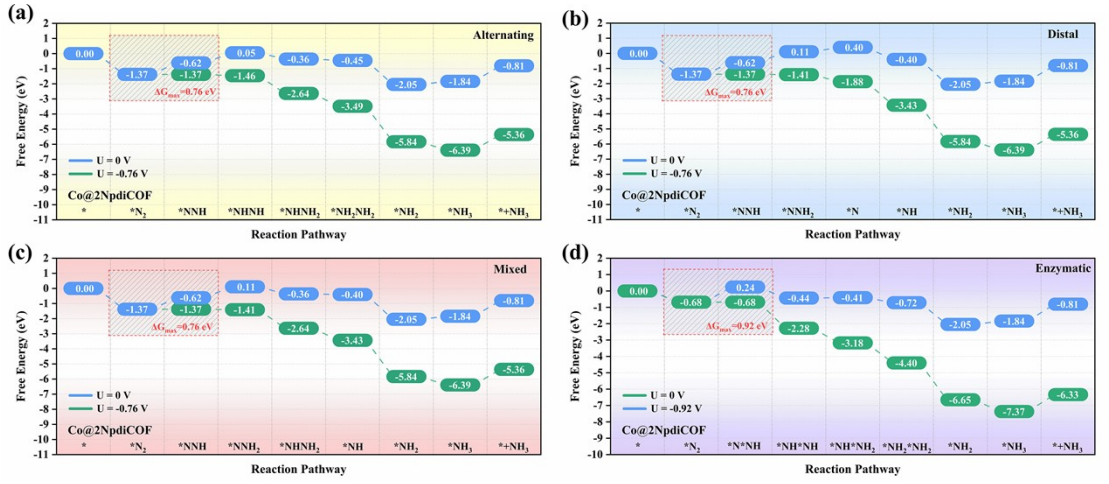

Figure S16. Free energy diagram of Co@2NpdiCOF in NRR along (a) Alternating pathway, (b) Distal pathway, (c) Mixed pathway and (d) Enzymatic pathway.

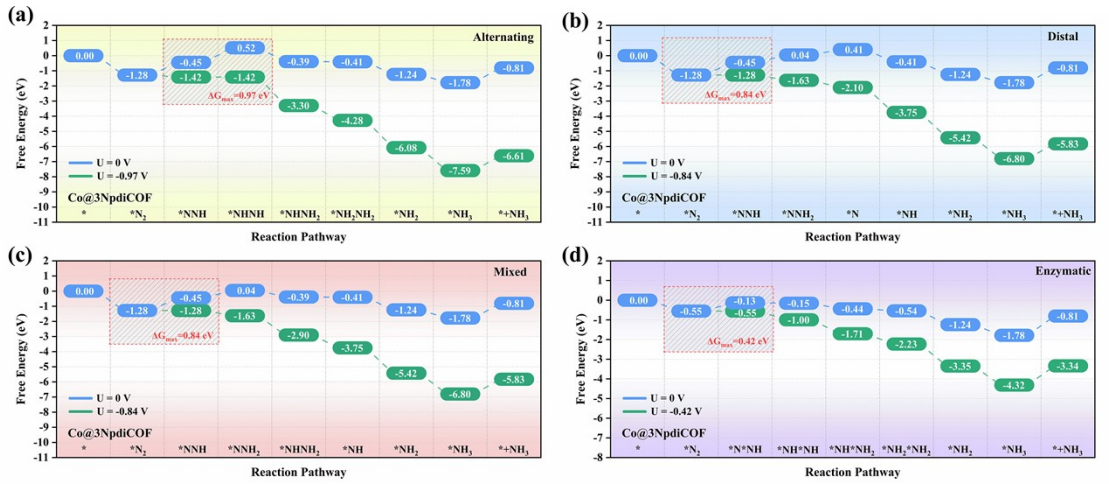

Figure S17. Free energy diagram of Co@3NpdiCOF in NRR along (a) Alternating pathway, (b) Distal pathway, (c) Mixed pathway and (d) Enzymatic pathway.

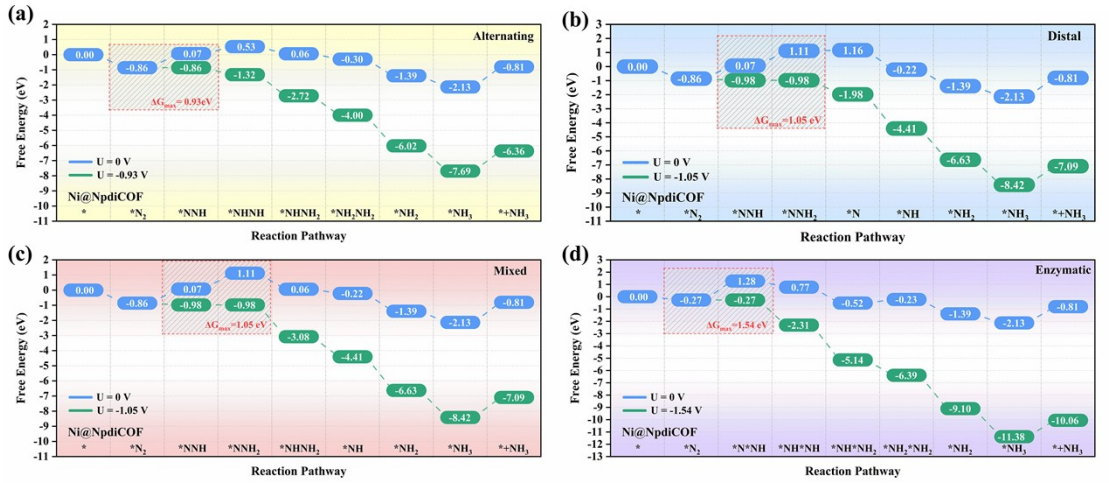

Figure S18. Free energy diagram of Ni@NpdiCOF in NRR along (a) Alternating pathway, (b) Distal pathway, (c) Mixed pathway and (d) Enzymatic pathway.

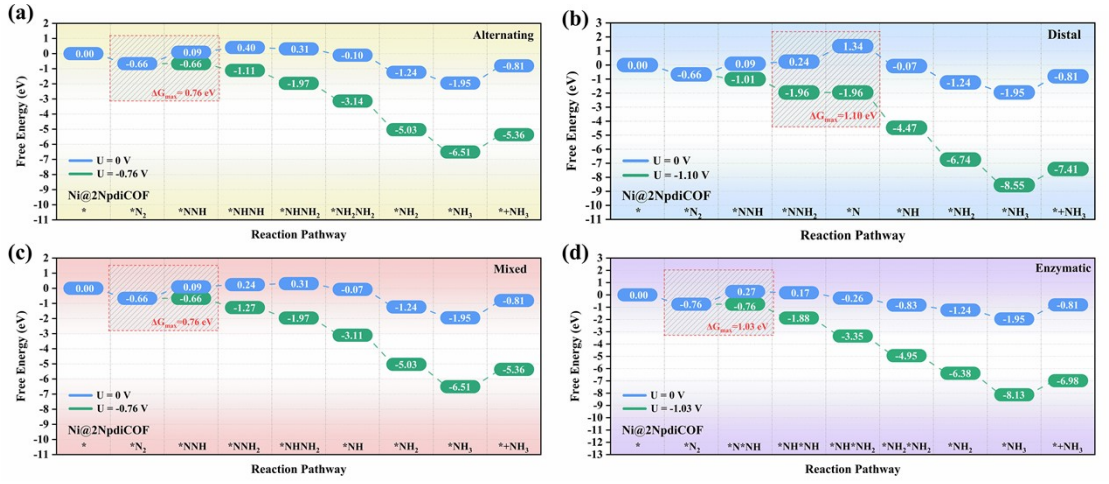

Figure S19. Free energy diagram of Ni@2NpdiCOF in NRR along (a) Alternating pathway, (b) Distal pathway, (c) Mixed pathway and (d) Enzymatic pathway.

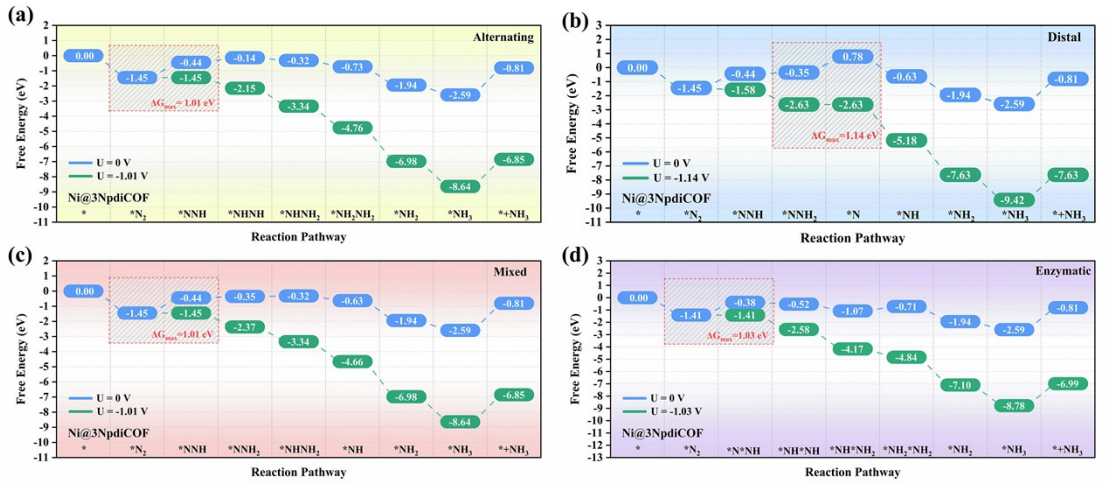

Figure S20. Free energy diagram of Ni@3NpdiCOF in NRR along (a) Alternating pathway, (b) Distal pathway, (c) Mixed pathway and (d) Enzymatic pathway.

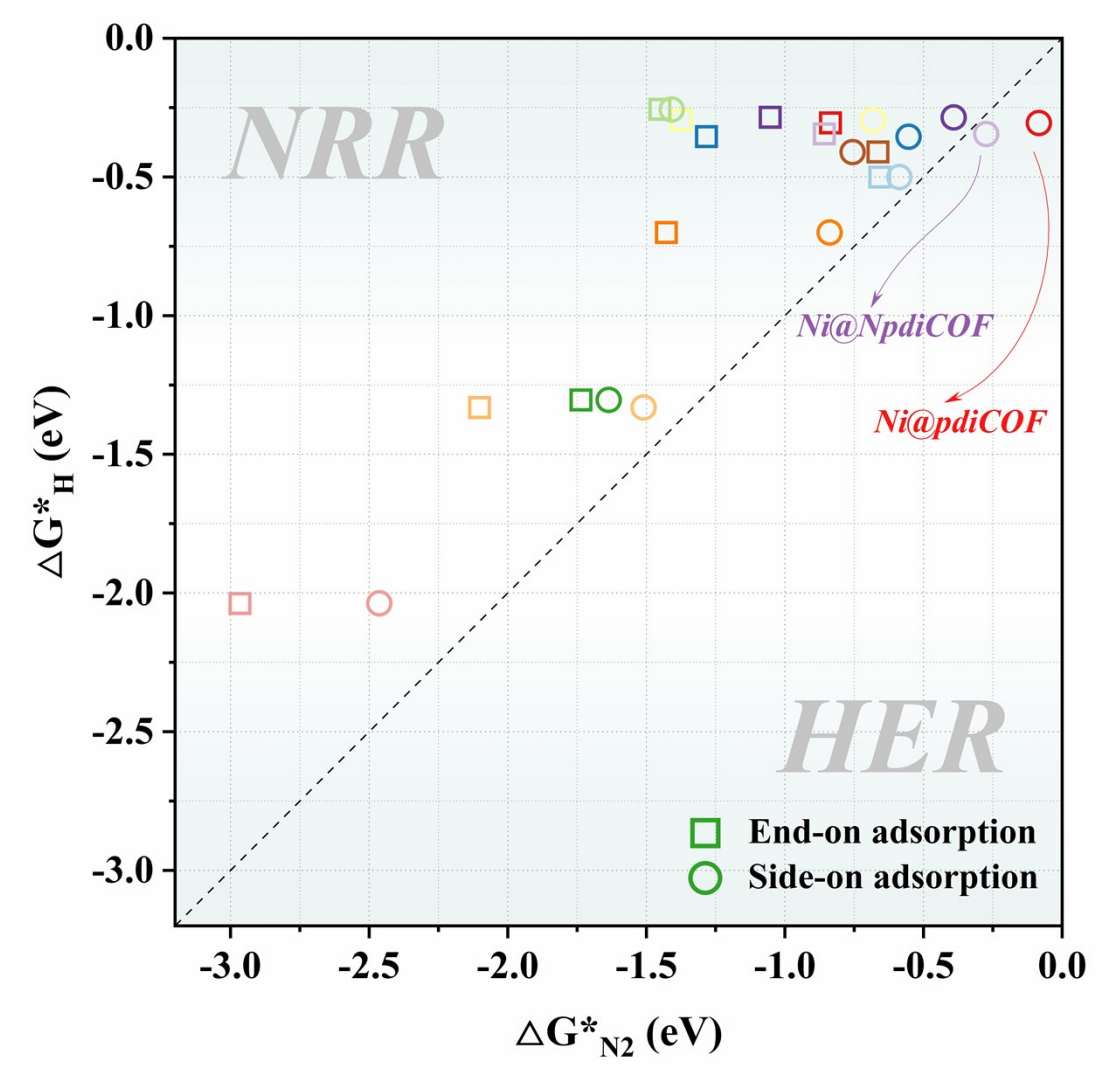

Figure S21. Adsorption energies for H and N_2 on different catalysts under two adsorption modes.

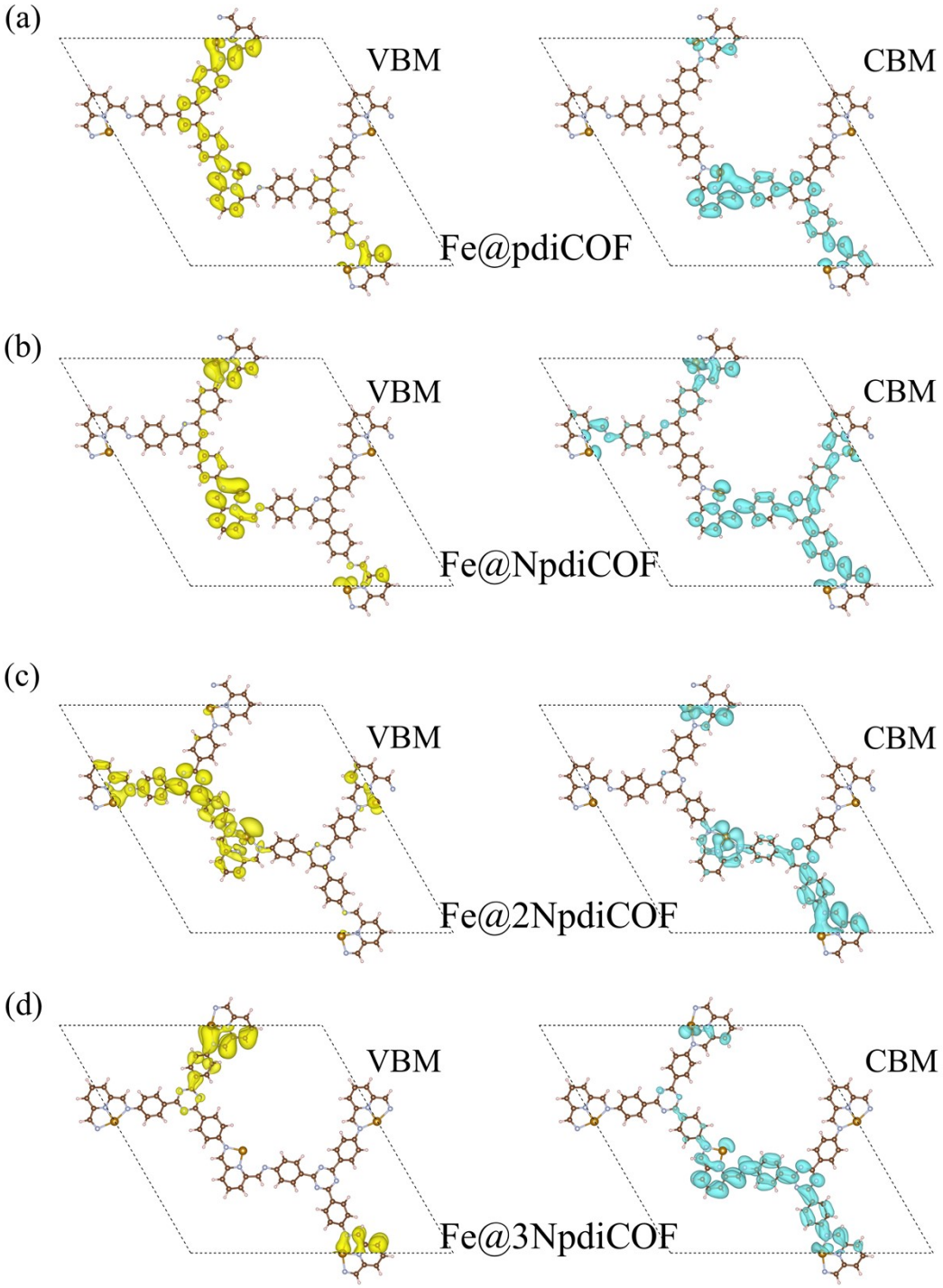

Figure S22. Spatial distribution of the valence band (VBM) and conduction band (CBM) with a valence of $2e^{-12}$ $Å^{-3}$ for (a) Fe@pdiCOF, (b) Fe@NpdiCOF, (c) Fe@2NpdiCOF, and (d) Fe@3NpdiCOF.

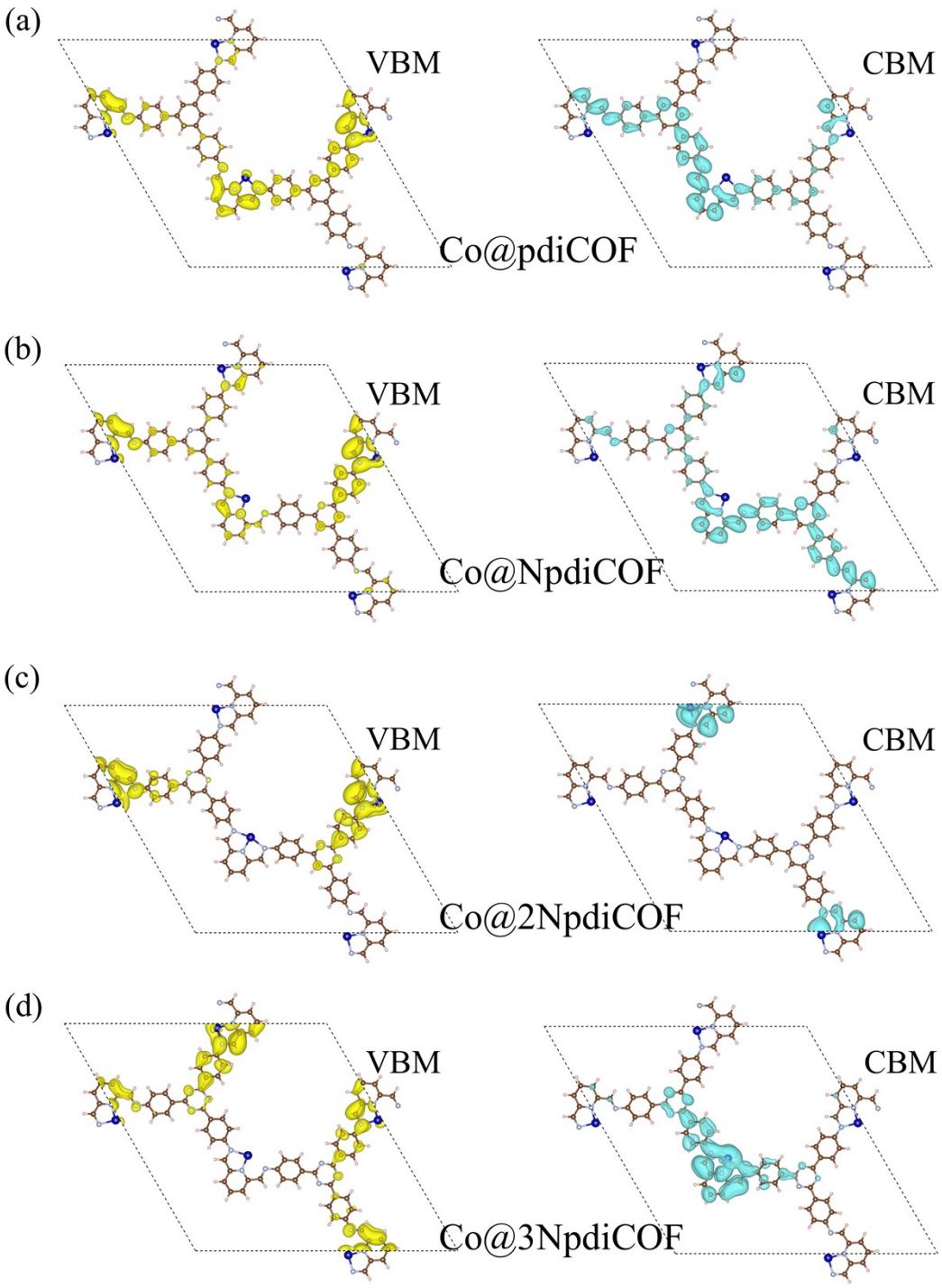

Figure S23. Spatial distribution of the valence band (VBM) and conduction band (CBM) with a valence of $2e^{-12}$ $Å^{-3}$ for (a) Co@pdiCOF, (b) Co@NpdiCOF, (c) Co@2NpdiCOF, and (d) Co@3NpdiCOF.

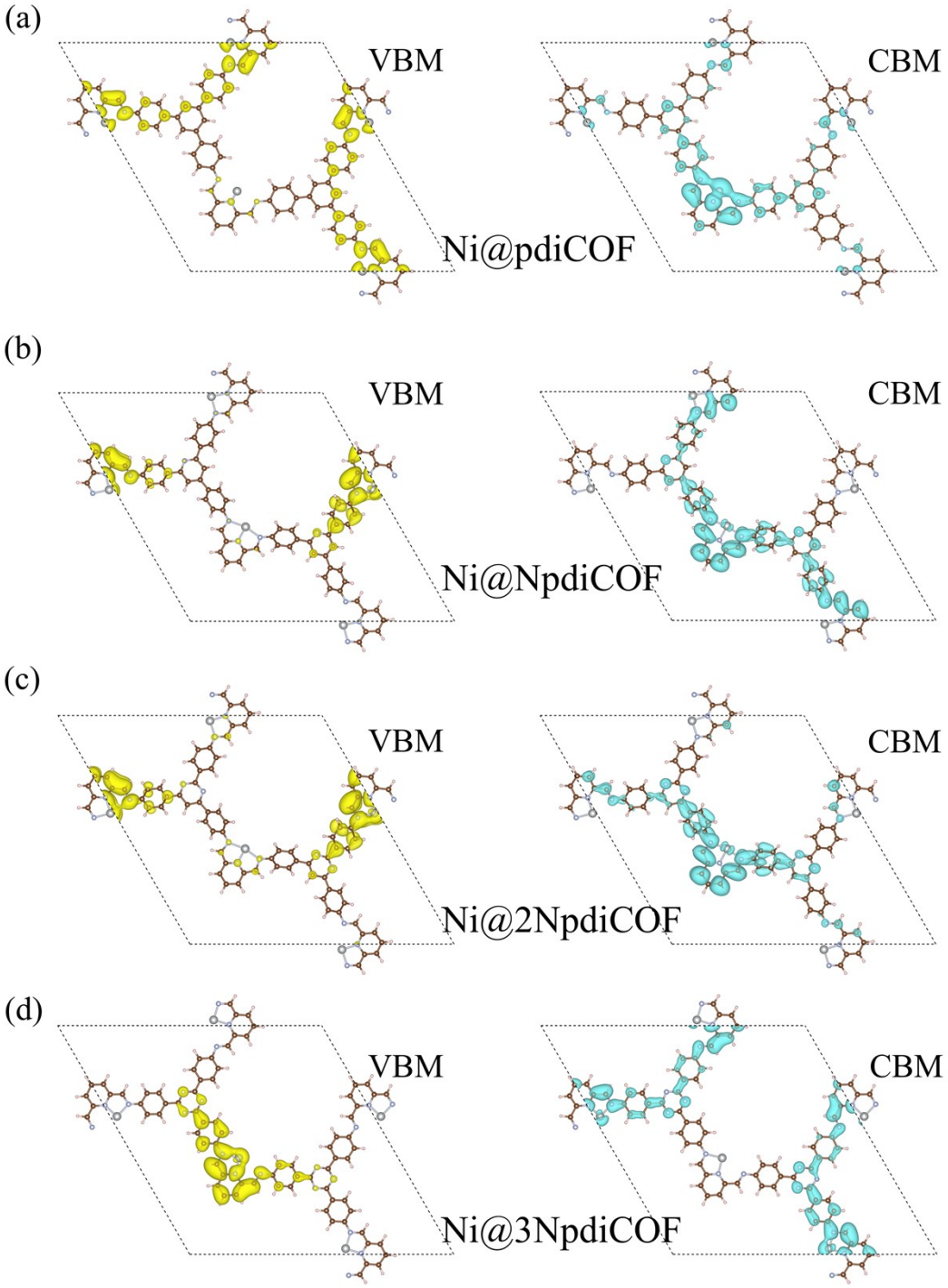

Figure S24. Spatial distribution of the valence band (VBM) and conduction band (CBM) with a valence of $2e^{-12}$ $Å^{-3}$ for (a) Ni@pdiCOF, (b) Ni@NpdiCOF, (c) Ni@2NpdiCOF, and (d) Ni@3NpdiCOF.

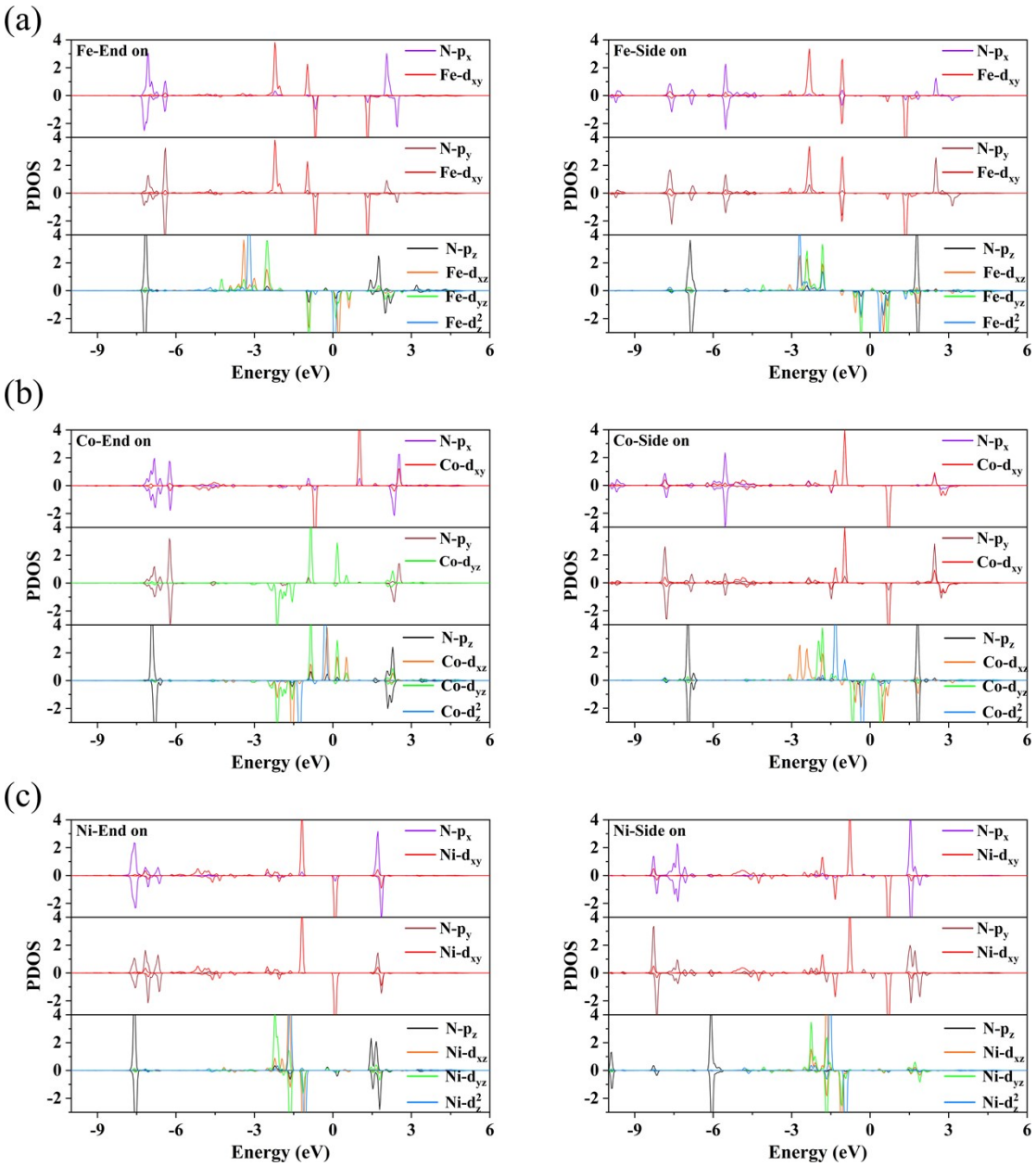

Figure S25 Projected DOS of nitrogen adsorption on different catalysts: (a) Fe@pdiCOF, (b) Co@pdiCOF, (c) Ni@pdiCOF.

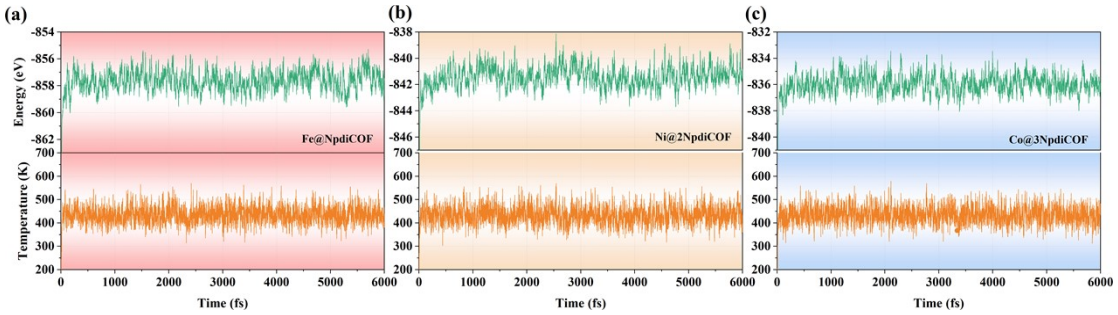

Figure S26 The changes of energy and temperature versus the AIMD simulation time for Fe@NpdiCOF (a), Ni@2NpdiCOF (b) and Co@3NpdiCOF (c).

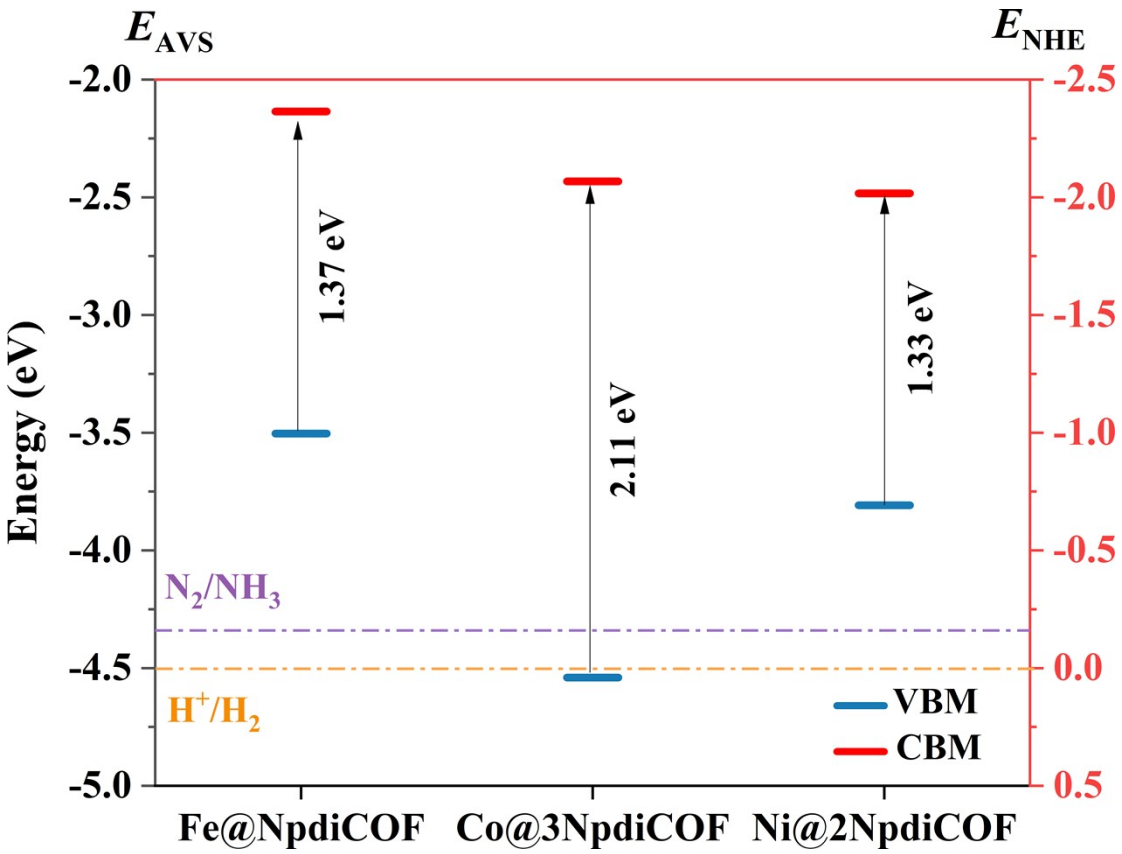

Figure S27 Theoretical energy position of the VBM and CBM of COFs relative to the absolute vacuum scale (E_{AVS}) and normal hydrogen electrode (E_{NHE}).

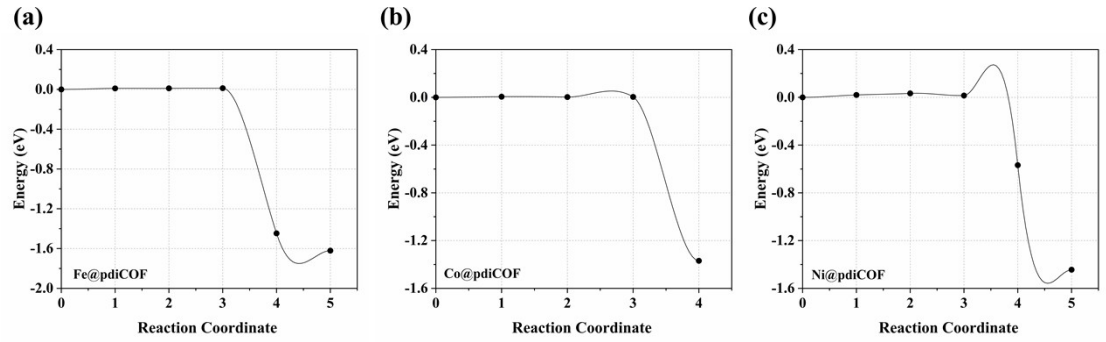

Figure S28 The CI-NEB transition state for the first hydrogenation step of the catalyst: (a) Fe@pdiCOF, (b) Co@pdiCOF and (c) Ni@pdiCOF

Reference:

1. J. Wang, Z. Zhang, Y. Li, Y. Qu, Y. Li, W. Li and M. Zhao, ACS Applied Materials & Interfaces, 2022, 14, 1024-1033.
2. W.-q. Hong, Z.-M. Ao and Y. Xu, Applied Physics Letters, 2024, 125.
3. R. Zhang, L. Jiao, W. Yang, G. Wan and H.-L. Jiang, Journal of Materials Chemistry A, 2019, 7, 26371-26377.
4. M. Zheng, H. Xu, Y. Li, K. Ding, Y. Zhang, C. Sun, W. Chen and W. Lin, The Journal of Physical Chemistry C, 2021, 125, 13880-13888.
5. D. Xu, B. Yan, Q. Liu, L. Zhang, J. Wang, G. Chen and Z. Cheng, Applied Surface Science, 2025, 692, 162726.
6. Y. Ma, T. Yang, H. Zou, W. Zang, Z. Kou, L. Mao, Y. Feng, L. Shen, S. J. Pennycook, L. Duan, X. Li and J. Wang, 2020, 32, 2002177.